# Initial Performance Results of the OMEGA Laser System

An important step in the U.S. inertial fusion effort toward demonstrating ignition and modest gain in the laboratory is the validation of high-performance direct-drive fusion capsules. The scientific program at UR/LLE[1] is aimed at studying near-ignition conditions in direct-drive capsules that achieve ion temperatures of 2 to 3 keV and fuel areal densities of 0.2 g/cm$^2$. Such capsules are expected to achieve convergence ratios greater than 20 and experience Rayleigh-Taylor (R-T) growth factors in excess of 500. The OMEGA laser system has been upgraded to demonstrate these near-ignition conditions. The system has now produced up to 37 kJ of UV energy on target in 60 beams. Ultimately, the system will provide versatile pulse shapes and produce high irradiation uniformity (1%–2%) on the capsule.

The preliminary design[2] for the upgraded OMEGA system was completed in October 1989. Detailed design commenced in October 1990. In December 1992, the 24-beam OMEGA laser fired its last shot before being decommissioned to allow for the construction of the upgraded system. Ten months later, the building modifications were completed and laser construction began. In January 1994, the pulse generation room (PGR) began operations, and, in April 1994, the entire driver was activated. The first full OMEGA beamline was completed in December 1994 and produced 800 J in the IR and 606 J in the UV. In February 1995, a single UV beam irradiated a target. In March, the first 60-beam laser shot was fired, and in April, all 60 beams irradiated a target. The final acceptance tests for the system were performed on 2 May 1995.

The acceptance criteria for the upgraded system were the demonstration of target irradiation with 30 kJ of UV energy in 60 beams with ~750-ps Gaussian pulses and the achievement of a beam-to-beam energy balance of 10% rms. This article provides a brief description of the laser system and then presents the initial system performance results that met and exceeded the acceptance criteria. Specifically, targets were irradiated with UV energies up to 37 kJ, and the beam-to-beam energy balance was better than 8%. Overall frequency-conversion efficiencies of 75% were routinely obtained. The full laser system was operated for 15 shots with a 1-h shot cycle, including nine consecutive target shots.

OMEGA is a Nd:glass laser in the master oscillator–power amplifier (MOPA) configuration (see Fig. 63.1). It uses rod amplifiers up to a beam diameter of 9 cm, followed by disk amplifiers up to an output aperture of 20 cm in the IR. Each amplifier is followed by a spatial filter. The 60 IR beams are expanded in the final spatial filters to a 28-cm aperture and converted to 351 nm using KDP crystals in the type II/type II polarization-mismatch frequency-tripling configuration developed at LLE.[3,4] The beams are uniformly distributed around a 3.3-m-diam target chamber and focused onto target with *f*/6 lenses. (The effective *f* number based on the beam diameter is approximately 6.7.) Details of the design and configuration of the laser system can be found in other LLE Review articles. In Ref. 5, an updated description of the system included design changes since the preliminary design.[2] More details were given in Ref. 6 (laser drivers and laser amplifiers), Ref. 7 (power conditioning, control systems, optomechanical systems, major structures, and the target area), Ref. 8 [the large-aperture ring amplifiers (LARA's)], and Ref. 9 (the final design review prepared for the Department of Energy). This article presents performance results for the driver, the power amplifiers, frequency conversion, the harmonic energy diagnostic system, the temporal laser pulse shape, and the target-bay alignment and pointing systems.

**Driver**

The OMEGA driver generates optical pulses that are amplified, frequency converted, and eventually irradiate the target. To provide precise control of the on-target irradiation for fusion experiments, the driver must provide a beam that is stable and appropriately shaped in space, time, and frequency. In the acceptance tests the amplitude stability of the OMEGA driver was demonstrated to be better than 2% rms.

Figure 63.2 depicts the configuration of the driver, which begins with a master oscillator that produces ~10-nJ, 80-ps Gaussian pulses at a rate of ~76 MHz. These pulses seed

feedback-stabilized regenerative amplifiers (regens), which produce ~0.5 mJ per pulse with a pulse width ranging from 0.5 ns to 5 ns. A pulse-shaping system, not yet implemented and not shown in Fig. 63.2, will temporally shape the master-oscillator pulses before injection into these regens. It will be possible to inject independent pulse shapes into each of the three regens (main pulse, foot pulse, and backlighter). For the acceptance tests described here, a Gaussian pulse of ~800-ps duration was produced using an etalon in the main-pulse regen. The pulse-shaping system and the foot-pulse and backlighter beams were not required.

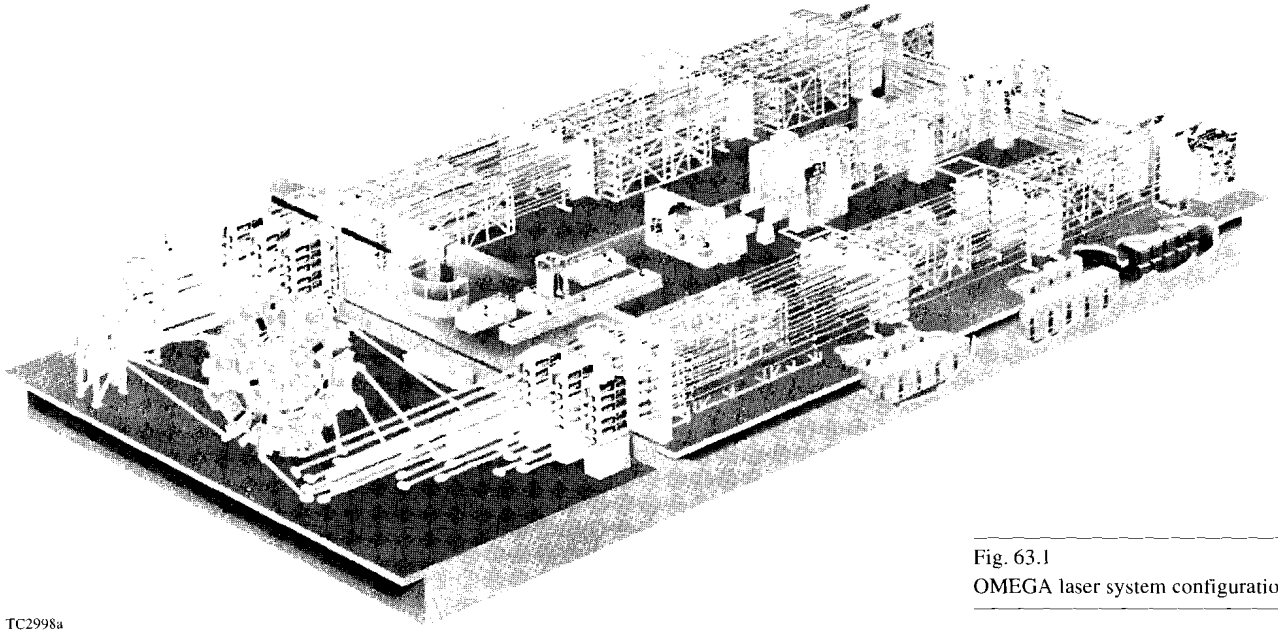

TC2998a

Fig. 63.1
OMEGA laser system configuration.

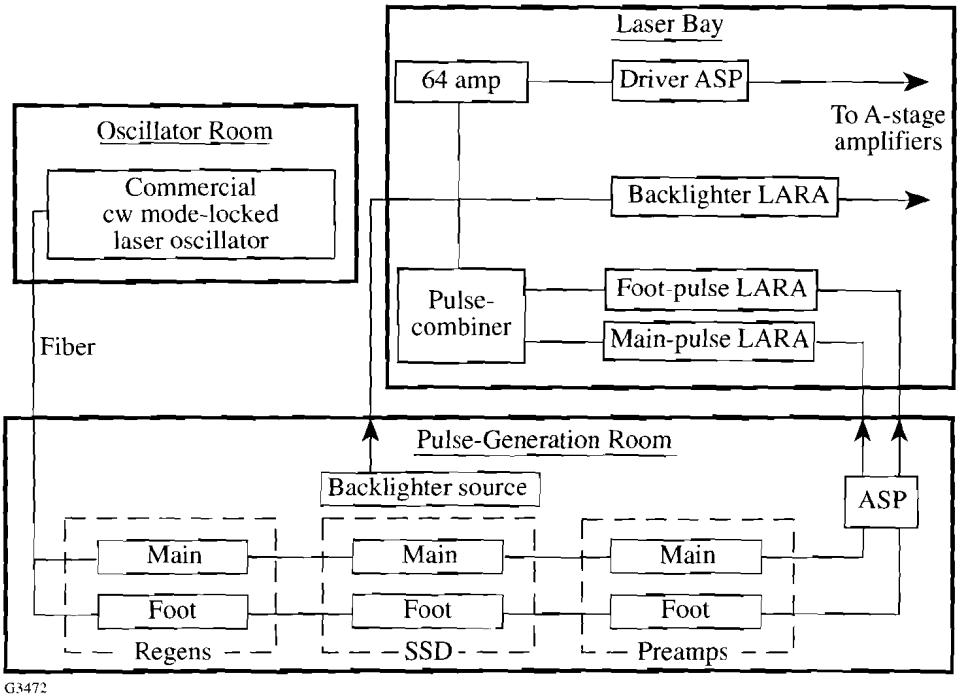


G3472

Fig. 63.2
Driver configuration for the OMEGA laser as used during the performance tests. Three optical pulses of independent temporal shapes (main, foot, and backlighter) can be generated in each of three separate drivers and subsequently amplified in three large-aperture ring amplifiers (LARA's).

The regens largely dictate the stability and reproducibility of the driver, which is why an amplitude feedback mechanism was implemented. This approach to stabilization has produced output pulses that have amplitudes and pulse widths with shot-to-shot variations of ≲1.5% rms. In addition, the time jitter between pulses from separate oscillators has been measured to be ≲30 ps rms. This low jitter permits the operation of synchronized oscillators for the main, foot, and backlighter pulses as well as ancillary oscillators/amplifiers to drive fiducials and probe beams needed for the diagnosis of fusion experiments. The wavelength of the pulses is monitored on every shot using Fabry-Perot interferometers that provide 0.05-Å wavelength resolution; care is taken to ensure that the wavelength remains constant to that accuracy so as not to compromise the frequency-conversion crystal (FCC) alignment.

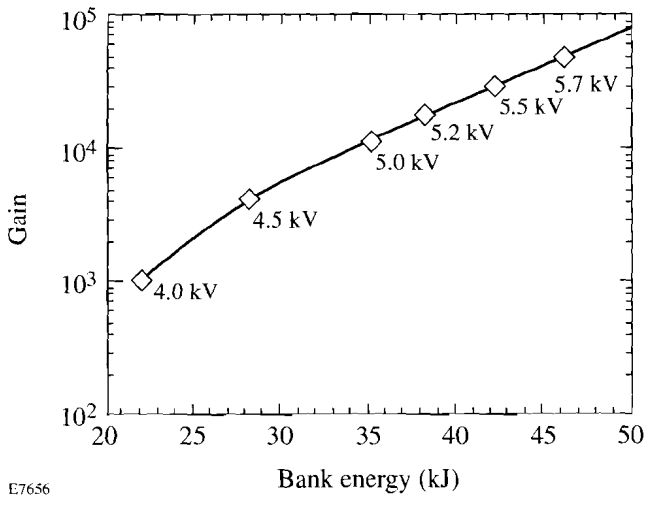


Fig. 63.3
Performance results for the main-pulse LARA. The gain is given as a function of bank energy for four-pass operation. The bank energy is determined from the charging voltage indicated.

To conserve space in the laser bay and enhance performance reliability, most of the driver gain is provided by a large-aperture ring amplifier (LARA). For the acceptance tests, LARA amplified the regen output from <1 mJ to ~1 J and a single-pass, 64-mm amplifier then amplified the pulse to ~5 J. LARA is a 40-mm, four-pass, imaging ring amplifier capable of producing energies ≳15 J in 1 ns. LARA is compact and fits easily on a 5-ft × 10-ft optical table. Figure 63.3 demonstrates the LARA gain performance in its four-pass configuration. Gains of up to ~$4 \times 10^4$ have been achieved. This performance largely exceeds current requirements and thus ensures that schemes to improve the irradiation uniformity, which require additional driver gain, can be accommodated without compromising the full output-energy performance of the system. The high quality of the output beam from LARA is clearly demonstrated by the near-field image and interferogram (Fig. 63.4) obtained during tests at full aperture (37 mm) for a pulse width of ~1 ns. The peak-to-valley phase distortion [Fig. 63.4(b)] was measured to be less than one wave at $\lambda = 1$ μm, while random intensity fluctuations were ≲10% rms. Under normal operating conditions on OMEGA, only the ~20-mm central region of the LARA aperture is used, resulting in ≲$\lambda/4$ phase error (peak to valley). The slight edge enhancement of the near-field image is due to the input beam apodizer that was designed for a lower output energy.

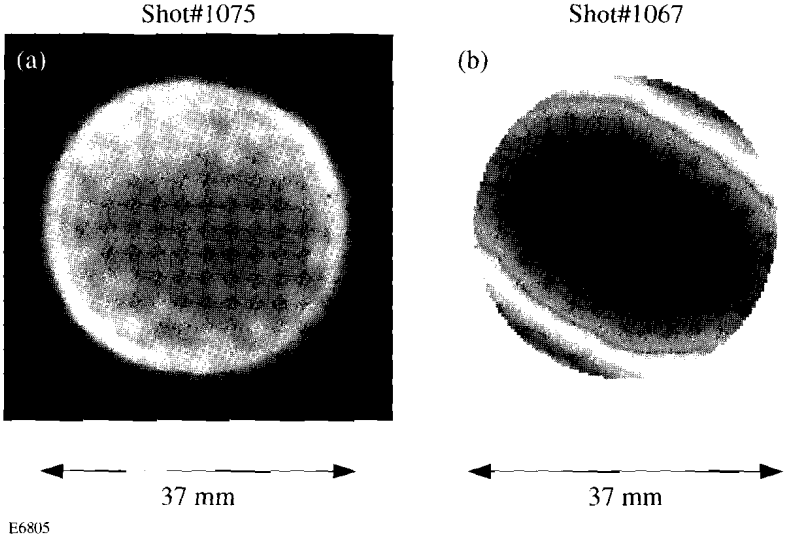


Fig. 63.4
(a) Near-field image and (b) interferogram of 37-mm-diam beams at the LARA output. The beam energy was 13.7 J in (a) and 17.8 J in (b).

The OMEGA driver is used to shape the output spatial profile of the laser (see Fig. 63.5). This is characterized by two features: the intensity profile and the location of the outer "edge" of the beam. (To maintain alignment and prevent modulations due to vignetting of the beam, an edge is needed to define the beam.) Each of these features is determined by the profile at an image plane in the driver that is relayed through the system by the spatial filters. To ensure high extraction efficiency in the disk amplifiers and high frequency-conversion efficiency, it is important that the output spatial profile of the laser be flat. The input beam profile must therefore compensate for the radial gain variation exhibited by the rod amplifiers of the system (stages A through D). This is done by placing a serrated apodizer[10] at the input to LARA and irradiating it with an appropriately sized beam from the PGR. Using a laser propagation code (*RAINBOW*) and the measured radial-gain profiles of each class of amplifier (40, 64, and 90 mm), the apodizer transmittance and input beam size have been designed to produce the desired beam intensity profile at the output of the system (the solid line of Fig. 63.5). For the tests reported here, the apodizer was used to shape the spatially Gaussian beam from the PGR. The beam edge is set entirely by the transmittance of the apodizer. The LARA spatial filter removes the high spatial frequencies created by the serrations while preserving the desired low-frequency beam shape. As a consequence, the pinhole in this filter is the tightest in the whole laser system—just five times the diffraction-limited size for its 2.0-cm beam.

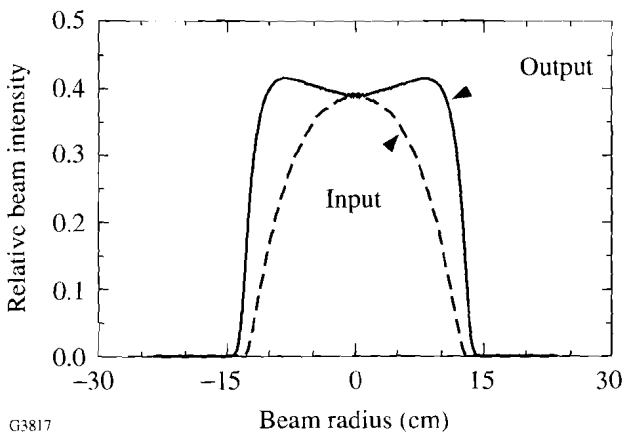


Fig.63.5
One-dimensional lineouts of the IR spatial intensity profile at the input to the amplifier chain (dashed line, scaled with the beamline paraxial magnification) and at the output of the final (stage-F) spatial filter (solid line). The input profile is strongly center-peaked to compensate for the radial gain profiles in the rod amplifiers.

**Power Amplifiers**

The OMEGA system has been designed to propagate the complex temporal pulse shapes required for direct-drive targets.[11] The system is staged for equivalent Gaussian pulse widths in the range of 0.5–3.0 ns. The 0.5-ns pulses are sufficiently short that it has been necessary to emphasize high gain in order to minimize B-integral effects.[12] For 3.0-ns pulses, on the other hand, the performance is limited by the damage fluences.

A staging diagram of the OMEGA laser is shown in Fig. 63.6. Values are given for the energy, fluence, and accumulated B-integral at various points for a 750-ps, temporal-Gaussian, spatially flat-topped pulse. Circular polarization is propagated through all of the 64- and 90-mm rod amplifiers to reduce non-azimuthally symmetric (i.e., "Maltese cross") beam modulation due to component birefringence (particularly in the rods), to reduce the B-integral in the rods,[13] and to reject retroreflections from optical components at the circular polarizers.[14] The laser performance used for the acceptance tests was approximately as shown in Fig. 63.6.

The beam splitting necessary to produce the requisite 60 beams is performed using a combination of wave plates and polarizing beam splitters. The first split is the stage-A split, in which the driver is split into three beams before the A amplifiers. The other splits are similar, except for the number of output beams, and will not be described in detail. The input to the stage-A splitter is first repolarized by a liquid-crystal circular polarizer[14] to eliminate changes in the split ratio in the event that the input polarization were to change. The input beam is then converted to linear polarization by an adjustable quarter-wave plate followed by a polarizing beam splitter that divides the beam into a high-contrast $p$-polarized beam and an $s$-polarized beam containing a small amount (<4% of the input intensity) of residual $p$-polarization. The $p$-polarized beam constitutes one of the three split outputs. The $s$-polarized beam passes through an adjustable half-wave plate and is split two ways by another polarizing beam splitter, forming the remaining two output beams. Each of the three output beams is reconverted to circular polarization by a rotatable quarter-wave plate and repolarized by another circular polarizer before leaving the split. The optical paths in the legs of the split are equalized to maintain relative beam timing. All mirror and beam-splitter reflections are kept in the same plane.

For the acceptance tests, the input energy to the A split was ~5 J. Each of the resulting three beams was amplified by a

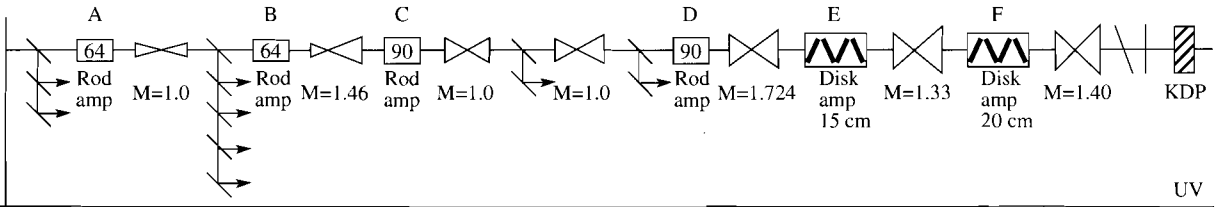


| | | | | | | | | | | | | | | | | | | |
|---|---|---|---|---|---|---|---|---|---|---|---|---|---|---|---|---|---|---|
| Energy (J) | 1.1 | 12.0 | 11.7 | 2.0 | 21.2 | 20.7 | 103 | 99.4 | 48.2 | 47 | 22.0 | 124 | 118 | 402 | 398 | 1040 | 978 | 750 |
| Avg. fluence ($J/cm^2$) | 0.1 | 0.87 | 0.85 | 0.15 | 1.3 | 0.56 | 2.3 | 2.2 | 1.1 | 1.0 | 0.48 | 2.3 | 0.71 | 2.5 | 1.35 | 3.5 | 1.7 | 1.4 |
| B-integral (radians) | 0.26 | 0.46 | 0.5 | 0.5 | 0.79 | 0.83 | 1.5 | 1.7 | 1.7 | 1.8 | 1.9 | 2.5 | 2.6 | 2.9 | 3.0 | 3.5 | 3.8 | ---- |

G3578

Fig. 63.6
Staging diagram of an OMEGA beamline through stages A–F (not to scale) for an input Gaussian pulse of 0.82-ns FWHM.

factor of 10 by a 64-mm-diam, stage-A rod amplifier (with a 61-mm clear aperture). After spatial filtering, each of these beams was split vertically into five beams in the stage-B split, for a total of 15 beams with ~3 J per beam. This provided adequate drive for the subsequent 64-mm and 90-mm rod-amplifier combination (stages B and C) located in each of the 15 beamlines to produce ~100 J at the final, four-way, stage-C split. (This is essentially identical to a beamline of the old OMEGA system where a 2-J drive in each of 24 beamlines produced just over 100 J at the output.) The final three amplifiers in each beamline in the upgraded system (the stage-D rods and the disk amplifiers of stages E and F) generate 97% of the system output energy for a 0.7-ns pulse. A drive of 22 J at the stage-D rod produces over 1 kJ of IR energy at the output of the stage-F amplifier.

## Frequency Conversion

The IR output of OMEGA is frequency tripled to 351 nm using two type-II KDP crystals per beam.[3,4] To guarantee high harmonic conversion it is necessary to maintain the proper phase-matching angles in the crystals. This requires precise control of the crystal orientation, the beam wavelength, and the crystal temperature. In addition, to ensure the optimum ratio of fundamental and second harmonic in the second (tripler) crystal, high-contrast linear polarization is required at the input to the first (doubler) crystal. For this reason a large-aperture polarizer is placed in each beam just before the crystals. The wavelength of the driver is constantly monitored by diagnostics with 0.05-Å resolution, and care is taken to maintain a constant wavelength. The crystals are maintained at the ambient temperature of the laser bay, which is nominally controlled to ±0.5°F. Variations in crystal temperature will be actively compensated for by using empirical temperature-tuning curves, although this has not yet proven necessary.

Prior to the installation of the crystals, the peaks of the angle-tuning curves for the doublers and triplers were found by using an off-line tuning procedure that used one of the remaining two OMEGA drivers not required for system activation. Configured to produce 100-ps, 2-mJ pulses at 5 Hz, this driver irradiated frequency-conversion cells (including the doubler and tripler) with a weakly converging beam of about 1 cm in diameter [see Fig. 63.7(a)]. This produced a spread of angles that included the optimum phase-matching angle for each of the crystals.[15] By properly referencing the experimental setup, the tuning peaks and thus the correct orientations for the doubler and tripler crystals could easily be determined in a single 20-shot (4-s) exposure of a CCD camera. Figure 63.7(b) shows one such exposure. The central lobes of the characteristic $\text{sinc}^2(x)$ intensity distributions for the green from the doubler (band AB) and the UV from the tripler (band CD) intersect at the optimum tuning position (marked with an "x"). The other broad band across the image (EF) is produced by rays that are phase matched for doubling in the tripler. The broadness of the second-harmonic (green) bands results from the relative insensitivity of doubling to changes in the ray angle along the *o* axis of each crystal. The CCD image is produced by a combination of all three wavelengths, with greatest sensitivity to the UV. Thus, there are many bands parallel to AB corresponding to green side lobes in the doubler, mostly imperceptible in the image; however, whenever these lobes intersect the line CD, i.e., are phase-matched for tripling, the UV generated is evident as a series of elliptical images. These images are narrower in the tripler tuning direction (parallel to AB) than in

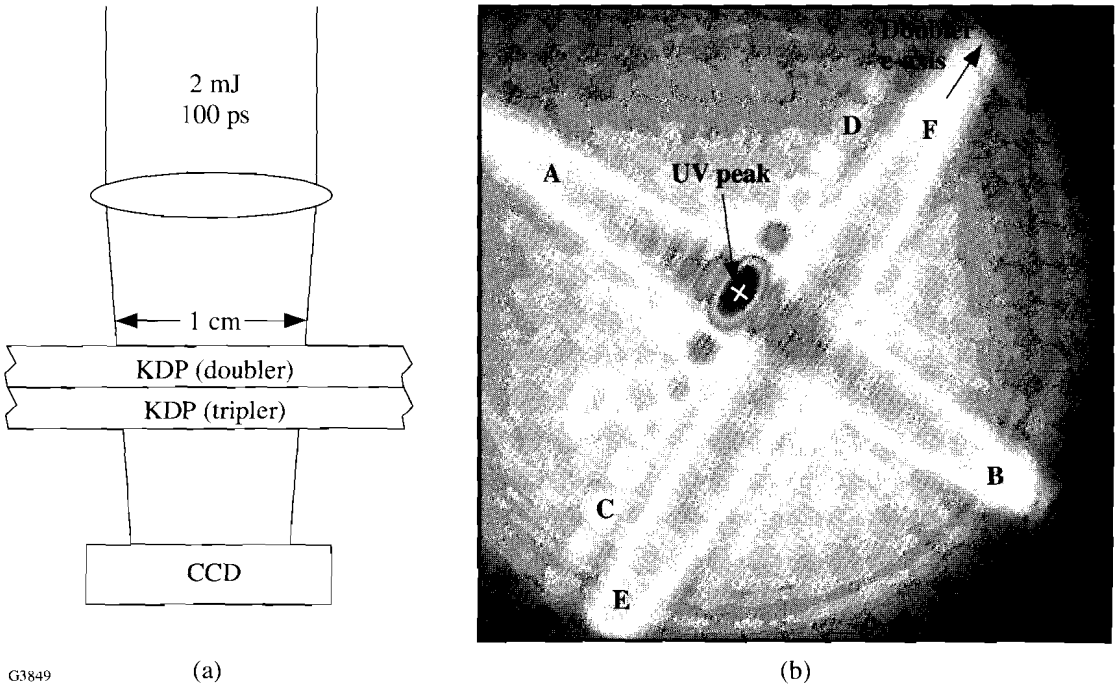


Fig. 63.7
(a) Off-line tuning technique for the frequency-conversion crystals (FCC's). A small-aperture (1-cm) beam is weakly focused through the FCC's onto a CCD camera; (b) resulting spatial pattern on the CCD. By identifying the ray in the converging beam that generates optimum UV, indicated by an "x," the necessary angle tilts of the FCC assembly in each of the two orthogonal directions may be determined. The arrow indicates the *e* axis of the doubler and the *o* axis of the tripler.

the doubler tuning direction (parallel to the arrow) because of the greater sensitivity of the tripler to the detuning angle.

The crystals were installed in the OMEGA system at the peak position as determined by the off-line tuning system. High-power angle-tuning scans were then performed about that position at 30% beam energy (300 J IR) with just three shots each for the doubler and tripler. In this procedure the doubling and tripling conversion efficiencies are fitted to the respective theoretical tuning curves, which are well represented as quadratic. The peak tuning positions were determined with a precision of ±50 μrad. The differences between the high-power peak tuning positions and those found from the off-line procedure were less than 125 μrad rms. This difference was presumed to be due mainly to a temperature differential between the off-line tuning setup and the location of the crystals in the OMEGA system. Even though no temperature compensation was applied to the crystal positions during high-power tuning, remarkably stable frequency-conversion efficiencies (70%–75%) were routinely achieved over a two-week period of activation shots. These results demonstrate the stability of the opto-mechanical alignment and the temperature control in the OMEGA facility.

Figure 63.8 is a plot of the $3\omega$ conversion efficiency versus the IR intensity incident on the crystals. The conversion efficiency is defined as the UV energy output from the crystals divided by the IR energy input to the crystals. The incident intensity is calculated using the input IR energy inferred from the energy measurement system, the IR beam profile shown in Fig. 63.5 (which has a nominal diameter of 27 cm), and the measured IR pulse width of 725 ps at the input to the crystals.

The achievement of frequency-conversion efficiencies greater than 70% is the result of a concerted effort to produce input IR beams that are highly suited for conversion. The beams have nearly flat intensity profiles with fill factors of ~90%. [The fill factor is the ratio of the integral of the actual beam shape to that of a flat (i.e., ideal) beam filling the clear aperture.] The intrinsic polarization purity of the disk amplifi-

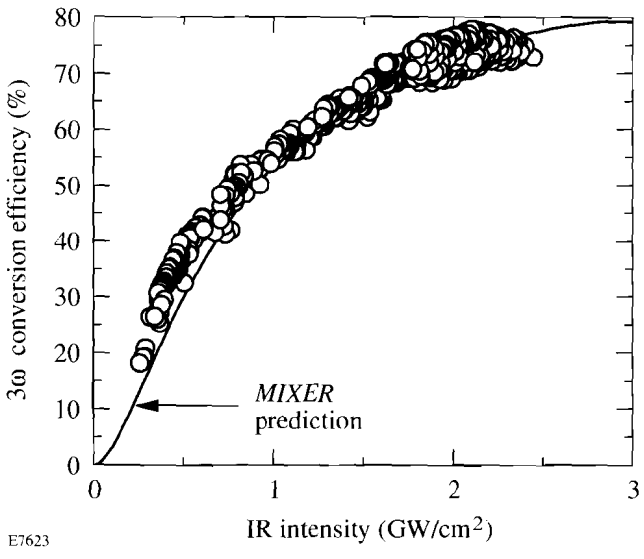


Fig. 63.8
Measured and predicted $3\omega$ energy conversion efficiency as a function of input IR intensity. The predictions take into account the experimental spatial profile of Fig. 63.5.

ers (depolarization <1% at any point in the clear aperture) and the low stress birefringence induced in the spatial-filter lenses produce beams that contain pure linear polarization with a contrast greater than 100:1 at all points in the clear aperture. The high-contrast linear polarizers (contrast of ~500:1) then produce beams that have a very high resultant contrast at the input to the crystals. Also, the laser was designed to produce high wavefront quality: in each beamline the accumulated B-integral is less than 4 radians (at 1 ns), and the optical tolerances are consistent with beams that are <1.4 times diffraction limited at 351 nm. (Measurements of the optical wavefront quality of OMEGA beamlines are planned for early FY96.)

The measured conversion efficiencies shown in Fig. 63.8 are generally in good agreement with predictions of the code *MIXER*.[4] However, some differences may be noted. In particular, the system seems to generate slightly more UV than predicted, especially at the lower intensities. One possible explanation is that the nonlinear coefficient $d_{36}/\varepsilon_0$ used in the code for Fig. 63.8 is a little too low. The value used for both crystals, $d_{36}/\varepsilon_0 = 0.39$ pm/V, is the same as that inferred from the experiments of Ref. 3 and subsequently accepted as standard.[16] (This value is quoted according to the now-agreed definition of Ref. 16, which is a factor of 2 lower than the definition used in Ref. 4, where $d_{36}/\varepsilon_0$ was quoted as 0.78 pm/V.) A higher value of $d_{36}$ in the tripler, which could be within the measurement error bounds of Ref. 3, would have the effect of shifting the theoretical curve to the left. The scatter in the experimental data probably reflects variations in the crystal temperatures, which were not compensated for during the acceptance tests, so it is the upper envelope of data points that should be compared with the theory. Also, variations in the laser spatial profile at differing input intensities and during the laser pulse have not been included. Additional experiments are needed to resolve the (minor) differences between prediction and experiment.

**System Output Energy**

To ensure optimal performance, the energy at the crystal output is measured at all three harmonic wavelengths—IR, green, and UV. This is performed with the harmonic energy diagnostics (HED's). The output (stage-F) alignment sensor package (F-ASP) for each beamline contains an optical pickoff that directs a fraction of the beamline energy (at all three wavelengths) to an integrating sphere for that beam. A single fiber optic samples the energy in the sphere and transports that signal to one of two HED's, where imaging spectrometers separate the three signals by wavelength. Each HED diagnoses 30 beams. In each HED, the 30 fibers are arranged such that, after dispersion, they form three $10 \times 3$ arrays, i.e., an image of every fiber in the IR, green, and UV. Figure 63.9 is a composite of the images from the two HED's for a single shot. Each of the beamlines, arranged in six ten-beam clusters, produces three images. The spatially integrated signal for each individual beam image is used as a measure of the energy in the beam at each wavelength. The HED's are calibrated by a full-aperture calorimeter located directly behind the F-ASP optical pickoff and at present provide energy measurements with an absolute accuracy (one standard deviation) of 2% and a relative accuracy of 1.9%. The relative accuracy is expected to improve to <1% in the near future. This system is described in detail in the following article.

The HED's were used to diagnose the beamline energy and overall beam balance for the acceptance tests. The system output energy was measured on numerous 60-beam shots, some of which were target shots. The system consistently produced >30 kJ with typical beam balances of 6%–8%. Figure 63.10 is a plot of the UV output energy versus the beamline IR energy at the crystal, including data for all beamlines for more than 20 shots. The data included some lower-energy shots produced during calibration and energy ramp-up procedures. The highest-energy 60-beam shot produced over 40 kJ of UV, and tests on an individual beam demonstrated that a beamline energy of 1 kJ IR can produce 750 J of UV. This is equivalent to a full-system output of 45 kJ UV, which, at 660 ps, corresponds to 68 TW.

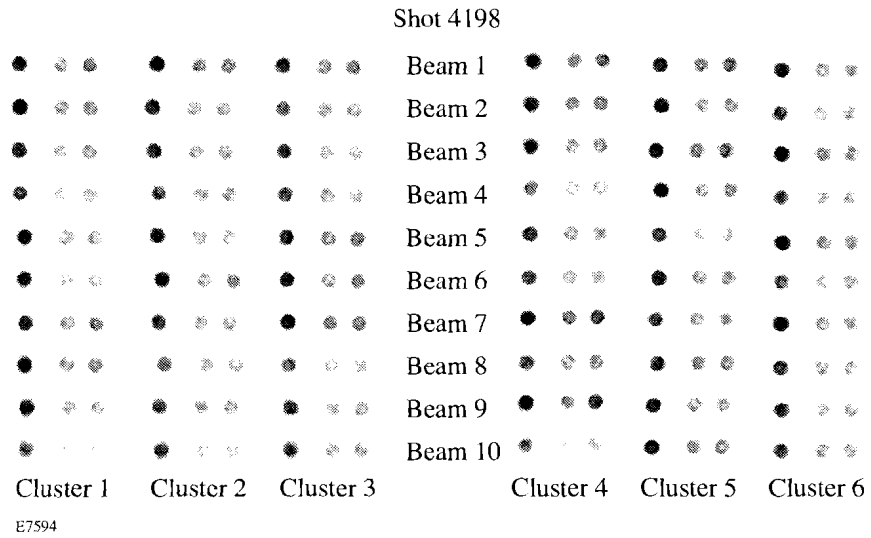


Fig. 63.9
Output of the harmonic energy diagnostic (HED) system. This produces images indicating the output energy at each of the UV, green, and IR wavelengths (from left to right) for each beam. A shot with the crystals detuned was used to illustrate the capability of the HED system—normally, very little signal is seen in the IR and green images.

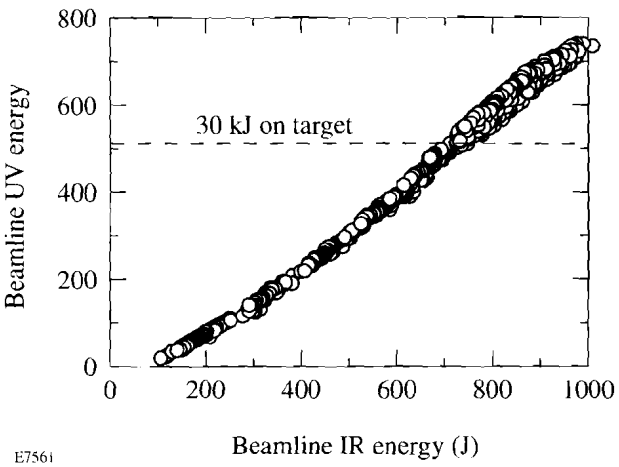


Fig. 63.10
Energy performance of the OMEGA laser. The UV energy at the FCC output is plotted against the IR energy at the FCC input for individual beams. The horizontal dashed line indicates the individual beam output energy required to produce a total energy on target of 30 kJ, taking into account transport losses from the FCC's to the target.

**Temporal Pulse Shape**

Figure 63.11 shows the temporal histories of the IR pulse at the input to the driver line and the output UV pulse measured on beam 45 on a shot in which 750 J of IR was produced at the input to the crystals. The steepened rise and slower falloff of the output pulse (compared with the input pulse) are caused by saturation effects in the amplifiers. The intensity dependence of frequency conversion results in the FWHM of the UV output pulse being shortened by about 10% with respect to the IR pulse at the input to the crystals. (At high conversion efficiency, the change in FWHM due to frequency conversion is minimal.) For a near-Gaussian pulse shape at the driver input, a 0.82-ns (FWHM) pulse is shortened to about 0.73 ns in the IR at the output of the last amplifier and to 0.66 ns in the UV.

The dashed curve in Fig. 63.11 is the predicted pulse shape from the laser propagation code *RAINBOW* when the measured input pulse shape is used as input to the code. This agreement indicates that the system meets the design specifications and performs as expected. Proper characterization of the system and normalization of the analysis tools are important for control of the on-target pulse shapes. Eventually, the laser propagation code will be used to propagate the desired on-target pulse shape backward through the system to determine the requisite driver pulse shape that must be produced by the pulse-shaping system. The good agreement seen in Fig. 63.11 provides confidence that accurate control of the on-target UV pulse shape will be possible.

Further verification of the accuracy of the code was provided by measurement of the pulse shape of the residual IR on a shot where the crystals were tuned (see Fig. 63.12). One curve is the signal as measured with a fast photodiode and oscilloscope, while the other is the residual IR predicted by the energy

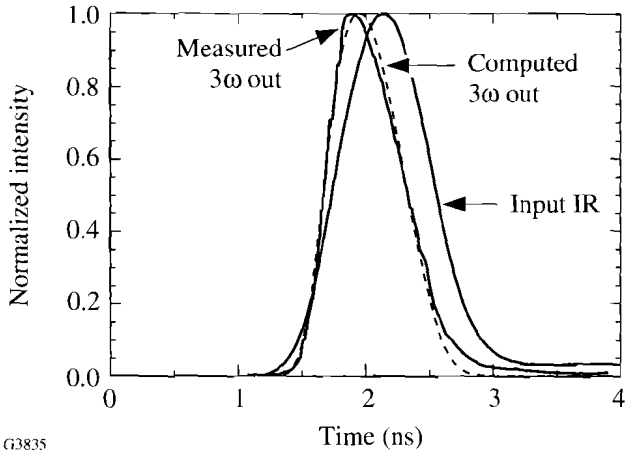


Fig. 63.11
Temporal pulse shapes measured at the input to the driver line and at the output of the FCC's. The measured output pulse shape is very close to that calculated by the propagation code *RAINBOW* (dashed curve).

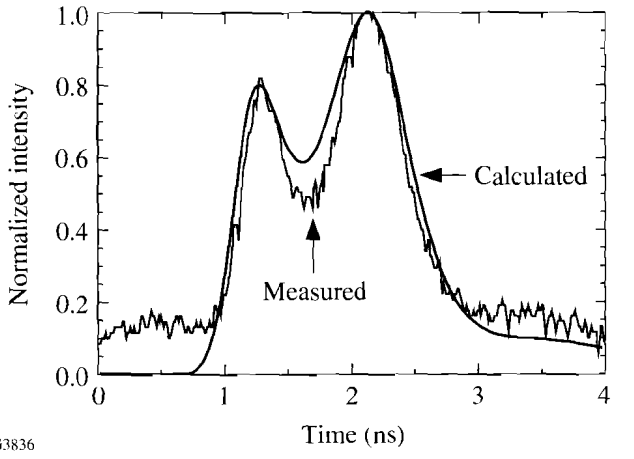


Fig. 63.12
Measured and predicted temporal pulse shape of the residual IR from a high-conversion shot, with 600 J of IR at the input to the FCC's. The *RAINBOW* prediction is shown as the smooth curve. The two peaks in time are associated with the intensity dependence of frequency conversion: maximum conversion, and thus a minimum in the residual IR, occurs at the peak of the pulse. The maximum residual IR intensity is ~13% of the maximum input IR intensity.

transport code *RAINBOW*. The two curves were normalized to match at the peak. The measured pulse shape has not been smoothed or had its pedestal removed. The predicted pulse shape was calculated by propagating the IR temporal pulse shape, measured at the input to the driver, through the driver, the system, and the frequency-conversion crystals. The calculated residual red output was then convolved with a falling-exponential (simple RC) approximation to the impulse response of the measurement's fast photodiode and oscilloscope to obtain the second plot. Even using this simple approximation, the major features of the data are replicated by the prediction. The central dip is due to the higher conversion efficiency at the center of the pulse, where conversion is maximum. The first peak is narrower than the second due to the steeper rise of the input IR pulse in comparison with its slower fall. The increased steepness of the leading edge is due to both a temporal asymmetry of the input to the driver and further steepening due to gain saturation. Since the conversion process responds essentially instantaneously for these time scales, the amplitudes of the two peaks are expected to be equal. Approximately 5% of the observed inequality is due to a change in the spatial pulse shape from early in the pulse to later times. The remainder is due to the convolution with the 180-ps impulse response of the diode and oscilloscope. The long, low intensity tail appearing in the calculation is due to an instrumental tail on the measured pulse shape used as the input to the code; its apparent agreement with the late-time background of the measured signal is fortuitous and of no significance.

## Target Irradiation Tests

Each of the 60 UV output beams from the laser is transported to the target chamber using two high-reflection UV mirrors, and then focused onto target with an *f*/6.4 aspheric lens. The beams are symmetrically distributed around the target chamber in the stretched soccer-ball geometry[2] with the beams located at the vertices of the hexagons and pentagons.

For the acceptance tests, large, gold-coated CH targets were irradiated with 60 beams. The targets were 1600-$\mu$m-diam solid plastic spheres, coated with 0.4 $\mu$m of gold, with an outer 4-$\mu$m layer of CH to reduce the x-ray flux. The resulting x rays were viewed with six pinhole cameras to provide verification of the positioning of all beams on target. Figure 63.13 shows two such images, viewing the target from opposing directions. The focus lenses were set to the surface-focus position, resulting in the relatively small spot sizes (<150-$\mu$m diameter).

The hexagonal/pentagonal configuration can be seen in Fig. 63.13. For this shot the pointing accuracy was 26 $\mu$m rms, dominated by a few beams with significant pointing errors. This result was achieved using only the cw alignment system; i.e., no adjustment of the beam alignment based on these x-ray pinhole images was performed during the acceptance tests.

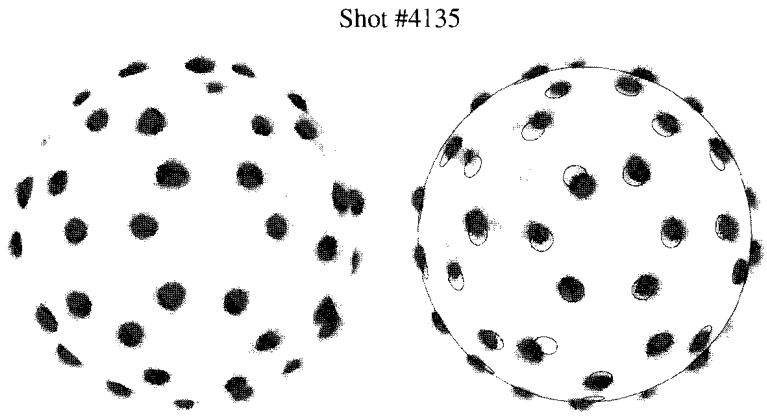


Fig. 63.13
Opposing x-ray pinhole images of a 1.6-mm-diam gold-coated target irradiated with 37 kJ in 60 tightly focused UV beams. The pentagonal and hexagonal patterns characteristic of the soccer-ball irradiation geometry are easily seen.

Significantly better pointing accuracy is expected when the alignment system is fully calibrated and between-shot feedback iterations are performed. Once calibrated, the maximum pointing error of any beam is expected to be less than 20 $\mu$m, which corresponds to 5% of the radius of a typical target. This accuracy will be more than sufficient for precision laser-fusion experiments, both direct drive and indirect drive.

**Future Work**

The project to upgrade the OMEGA laser system was aimed at creating a system that can be enhanced in various stages to meet the progressively more stringent demands of the planned fusion experiments. The achievement of 40 kJ of UV at ~7% beam balance, while exceeding system acceptance criteria, is only part of what will enhance the probability of success of the LLE experimental plan.[1] This plan calls for distributed phase plates (DPP's), two-dimensional smoothing by spectral dispersion (SSD), and initial pulse shaping (at ~20:1 contrast) to be implemented during FY96. These enhancements are expected to produce on-target irradiation with (rms) nonuniformities below ~5%. Ultimately, high-contrast pulse shaping (400:1), power balance control, and additional uniformity enhancements are needed to reduce nonuniformities below 2%, to enable OMEGA to be used for the implosion of high-performance capsules under near-ignition conditions.

**Conclusions**

The acceptance tests for OMEGA have demonstrated performance results that exceed requirements. The driver produces output pulses that are highly stable in amplitude, pulse width, and wavelength, resulting in stable and predictable performance of the entire laser system. Separate tests have also shown that the driver has the excess gain capability necessary for the future implementation of SSD and pulse shaping.

The OMEGA laser has produced over 40 kJ in the UV and has irradiated targets with up to 37 kJ with <8% rms imbalance in the energies of the 60 beams. The consistent achievement of high frequency-conversion efficiency (~75%) is indicative of good beam quality and control of the various beam and crystal parameters. The consistency of this performance over many days of operation is proof of the overall optomechanical stability of the system. Also, a 15-shot series including nine consecutive target shots has demonstrated the 1-h shot cycle that is necessary for a productive experimental program.

OMEGA is now a well-characterized system that performs above specifications. Once the planned enhancements for the control of pulse shape and uniformity are in place, the system will be uniquely capable of conducting precision direct- and indirect-drive fusion experiments.

## ACKNOWLEDGMENT

This work was supported by the U.S. Department of Energy Office of Inertial Confinement Fusion under Cooperative Agreement No. DE-FC03-92SF19460, the University of Rochester, and the New York State Energy Research and Development Authority. The support of DOE does not constitute an endorsement by DOE of the views expressed in this article.

## REFERENCES

1. OMEGA Upgrade Program Plan, University of Rochester, Laboratory for Laser Energetics (May 1994).
2. R. S. Craxton, ed., *OMEGA Upgrade Preliminary Design*, Laboratory for Laser Energetics Report DOE/DP 40200-101, University of Rochester (1989).
3. W. Seka, S. D. Jacobs, J. E. Rizzo, R. Boni, and R. S. Craxton, Opt. Commun. **34**, 469 (1980).
4. R. S. Craxton, IEEE J. Quantum Electron. **QE-17**, 1771 (1981).

5. Laboratory for Laser Energetics LLE Review **55**, NTIS document No. DOE/DP/40200-257, 1993 (unpublished), p. 178.

6. Laboratory for Laser Energetics LLE Review **56**, NTIS document No. DOE/DP/40200-277, 1993 (unpublished), p. 225.

7. Laboratory for Laser Energetics LLE Review **57**, NTIS document No. DOE/SF/19460-02, 1993 (unpublished), p. 32.

8. Laboratory for Laser Energetics LLE Review **58**, NTIS document No. DOE/SF/19460-17, 1994 (unpublished), p. 90.

9. T. R. Boehly, Ed., *OMEGA Upgrade Project Final Design Review* (KD3′), September 1993.

10. D. R. Speck, Lawrence Livermore National Laboratory Laser Program Annual Report 1988/89, UCRL-50021-88/89 (1993), pp. 4-10–4-12.

11. Proposal for Renewal Award for Cooperative Agreement DE-FC03-85-DP402000 (US DOE/LLE, October 1991), pp. 2.70–2.84.

12. D. C. Brown, in *High-Peak-Power Nd:Glass Laser Systems* (Springer-Verlag, New York, 1981), Vol. 7.7, pp. 227–235.

13. D. C. Brown, op. cit., p. 43.

14. S. D. Jacobs, K. A. Cerqua, T. J. Kessler, W. Seka, and R. Bahr, in *Laser Induced Damage in Optical Materials: 1984*, Nat. Bur. Stand. (U.S.) Spec. Publ. 727 (U.S. Government Printing Office, Washington, DC, 1984), p. 15.

15. W. L. Smith and T. F. Deaton, Lawrence Livermore National Laboratory Laser Program Annual Report 1979, UCRL-50021-79 (1980), p. 2-209.

16. D. Eimerl, Ferroelectrics **72**, 95 (1987).